Transient Analysis of Ferrite in Three-Dimensional Space

NAOYA KUKUTSU, NORINOBU YOSHIDA, MEMBER, IEEE, AND ICHIRO FUKAI, MEMBER, IEEE

Abstract—**The anisotropic medium has been applied to realize the nonreciprocal devices. The characteristics of these devices have become more advanced through the appearance of various materials and the miniaturization of the circuit created by the integration of circuits in MIC. In particular for microwave and millimeter-wave circuits, ferrite is a typical gyroanisotropic medium. So a significant amount of research and many analyses have been carried out to develop nonreciprocal devices using ferrite. To obtain more exact determinations of the properties of these devices, it is necessary to analyze three-dimensional space due to their complicated structures and the medium conditions. And recently, high-speed digital technology has been developed, so that it is important to analyze the electromagnetic field with time domain. This paper presents Bergeron's formulation of vector analysis for magnetized ferrite in a three-dimensional space and time domain. Results are provided for two cases with respect to the relative angle between the directions of the dc magnetic field and wave propagation. For both cases, the results are compared with analytical ones, and the validity of the formulation is verified.**

I. Introduction

THE ANISOTROPIC medium has been applied to realize such nonreciprocal devices as gyrators, isolators, and circulators for the microwaves, millimeter waves, and optical waves. The characteristics of these devices have become more advanced through the appearance of various materials and the integration of circuits in MIC, which has brought about miniaturization. In particular, for microwave and millimeter-wave circuits, ferrite is a typical gyroanisotropic medium. So a considerable amount of research and many analyses have been carried out to develop nonreciprocal devices using ferrite.

In the past, most of these studies have been performed using static and two-dimensional analyses. However, to determine more exactly the properties of these devices, it is necessary to analyze three-dimensional space because of the medium conditions, which involve the tensor permeability of ferrite and their complicated structures. Recently, high-speed digital technology has been developed and so it is important to analyze the electromagnetic field with time domain. In these studies, a unified formulation for both the boundary conditions and the characteristics of medium is indispensable for calculating exact total three-dimensional field responses in a time domain. Furthermore, the transient analysis of an electromagnetic field not only clarifies the variation of the field in time but also provides information on the mechanism by which the distribution of the electromagnetic field in the stationary state is brought about. However, the computations involving all these medium and boundary conditions by analytical methods are usually very complicated and difficult. Thus a numerical analysis method is required. The recent advances of the digital computer in both speed and memory capacity enable us to solve the equations for actual subjects. But conventional numerical methods are insufficient for the analyses in three-dimensional space and time domain.

Therefore a new method has been proposed for the transient analysis in the three-dimensional space. The method is based on the equivalent circuit of Maxwell's equation and a formulation by Bergeron's method (referred to here as the present method) [1], [2]. Useful results have been reported by making use of the characteristics of this method [3]–[6]. The present method has the characteristic that both voltage and current variables for each direction are assigned at each node in the lattice network. This property permits calculation of the effect of coupling between the magnetic fields, which is related to the off-diagonal elements of the permeability tensor. So the present method is useful for the analysis of nonreciprocal devices involving an anisotropic medium.

However, the finite difference time-domain method and the transmission line matrix method [7]–[9] do not have this merit, because of assignment of the single field variable at each node. For the two-dimensional space and time domain, the effect of ferrite has already been formulated by the present method [10]. In this paper, the formulation of the magnetized ferrite in the three-dimensional space and time domain is presented. The characteristics of the formulation are summarized as follows.

1) An anisotropic medium is assumed with the lumped elements in each node in the equivalent circuit of Maxwell's equation. The tensor permeability of the ferrite is then expressed as the equivalent inductances with mutual coupling.

2) The characteristic differential equation of the magnetized ferrite is formulated as the difference equation in time domain by using the trapezoidal rule.

In the following sections, the formulation of the magnetized ferrite by the present method is described in detail. Next, in discussing the validity of the formulation, results are presented for two cases with respect to the relative angle between the directions of the dc magnetic field and wave propagation. One is for the wavelength versus dc

Manuscript received March 5, 1987, revised July 30, 1987.

The authors are with the Department of Electrical Engineering, Hokkaido University, Sapporo, 060 Japan.

IEEE Log Number 8717583.

0018-9480/88/0100-0114$01.00 ©1988 IEEE

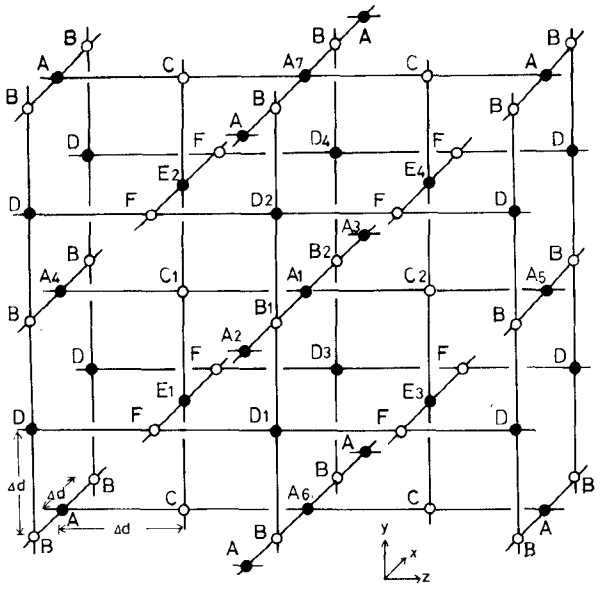

Fig. 1. Three-dimensional lattice network model of Maxwell's equation.

TABLE I
CORRESPONDENCE BETWEEN THE FIELD VARIABLES IN MAXWELL'S EQUATION AND THE EQUIVALENT CIRCUIT AT EACH KIND OF NODE IN THE EQUIVALENT CIRCUIT

	Electric node			Magnetic node	
	Maxwell's equations	Variables		Maxwell's equations	Variables
A k	$\frac{\partial Hx}{\partial z}-\frac{\partial Hz}{\partial x}=\varepsilon_0\frac{\partial Ey}{\partial t}$	$Vy \equiv Ey$	F k	$\frac{\partial Ex}{\partial z}-\frac{\partial Ez}{\partial x}=-\mu_0\frac{\partial Hy}{\partial t}$	$V_y^* \equiv Hy$
	$-\frac{\partial Ey}{\partial z}=-\mu_0\frac{\partial Hx}{\partial t}$	$Iz \equiv -Hx$		$-\frac{\partial Hy}{\partial z}=\varepsilon_0\frac{\partial Ex}{\partial t}$	$I_z^* \equiv Ex$
	$\frac{\partial Ey}{\partial x}=-\mu_0\frac{\partial Hz}{\partial t}$	$Ix \equiv Hz$		$\frac{\partial Hy}{\partial x}=\varepsilon_0\frac{\partial Ez}{\partial t}$	$I_x^* \equiv -Ez$
D k	$\frac{\partial Hz}{\partial y}-\frac{\partial Hy}{\partial z}=\varepsilon_0\frac{\partial Ex}{\partial t}$	$Vx \equiv Ex$	B k	$\frac{\partial Ey}{\partial x}-\frac{\partial Ex}{\partial y}=-\mu_0\frac{\partial Hz}{\partial t}$	$V_z^* \equiv Hz$
	$\frac{\partial Ex}{\partial z}=-\mu_0\frac{\partial Hy}{\partial t}$	$Iz \equiv Hy$		$\frac{\partial Hz}{\partial y}=\varepsilon_0\frac{\partial Ex}{\partial t}$	$I_y^* \equiv -Ex$
	$-\frac{\partial Ex}{\partial y}=-\mu_0\frac{\partial Hz}{\partial t}$	$Iy \equiv -Hz$		$-\frac{\partial Hz}{\partial x}=\varepsilon_0\frac{\partial Ey}{\partial t}$	$I_x^* \equiv Ey$
E k	$\frac{\partial Hy}{\partial x}-\frac{\partial Hx}{\partial y}=\varepsilon_0\frac{\partial Ez}{\partial t}$	$Vz \equiv -Ez$	C k	$\frac{\partial Ez}{\partial y}-\frac{\partial Ey}{\partial z}=-\mu_0\frac{\partial Hx}{\partial t}$	$V_x^* \equiv -Hx$
	$\frac{\partial Ez}{\partial y}=-\mu_0\frac{\partial Hx}{\partial t}$	$Iy \equiv -Hx$		$\frac{\partial Hx}{\partial z}=\varepsilon_0\frac{\partial Ey}{\partial t}$	$I_z^* \equiv Ey$
	$\frac{\partial Ez}{\partial x}=-\mu_0\frac{\partial Hy}{\partial t}$	$Ix \equiv Hy$		$-\frac{\partial Hx}{\partial y}=\varepsilon_0\frac{\partial Ez}{\partial t}$	$I_y^* \equiv -Ez$
dielectric constant	$C_0=\varepsilon_0/2$		dielectric constant	$L_0^*=\varepsilon_0/2$	
permeability	$L_0=\mu_0/2$		permeability	$C_0^*=\mu_0/2$	
polarization	$\Delta C=\varepsilon_0\chi_e/2\cdot\Delta d$		magnetization	$\Delta C^*=\mu_0\chi_m/2\cdot\Delta d$	
conductivity	$G=\sigma/2\cdot\Delta d$		magnetic current loss	$G^*=\sigma^*/2\cdot\Delta d$	
magnetization	$\Delta L=\mu_0\chi_m/2\cdot\Delta d$		polarization	$\Delta L^*=\varepsilon_0\chi_e/2\cdot\Delta d$	

magnetic field in a perpendicularly magnetized rectangular waveguide; the other is for the characteristics of Faraday effect, such as the phase constant and rotated angle in the longitudinally magnetized cylindrical waveguide. For both cases, the results are discussed along with analytical ones, and the validity of the formulation is presented.

II. Three-Dimensional Nodal Equation of Electromagnetic Field by Bergeron's Method

In the present method, the electromagnetic field is expressed in the equivalent circuit of the three-dimensional lattice network shown in Fig. 1. In this network, each set of two-dimensional equations for the propagation of waves in each plane is related to a node and connected lines. The line between nodes is a one-dimensional transmission line, and the node is a point where the continuity of current occurs. In this figure, Δd is the interval between adjacent nodes in the equivalent circuit. The black node ● stands for the electric node at which an electric field component is treated as a voltage variable, and the white node ○ stands for the magnetic node at which a magnetic field component is treated as a voltage variable. In Table I, the correlations between equivalent circuit variables and the field ones are shown at every kind of node in the network. All variables at the magnetic nodes are characterized by the symbol * because of the duality of their physical meaning, as compared with their interpretation at the electric node. The present method has the characteristic that both voltage and current variables for each direction are assigned at each node in the lattice network. This property enables us to calculate the effect of coupling between the magnetic fields, which is related to the off-diagonal elements of the permeability tensor.

III. Formulation of Ferrite

Girbert derived one differential form of phenomenological damping of ferrite that is often used. The equation of motion using the Girbert form of damping is written as

$$\frac{d\vec{M}}{dt}=-\gamma(\vec{M}\times\vec{H})+\frac{\alpha}{M}\left[\vec{M}\times\frac{d\vec{M}}{dt}\right] \tag{1}$$

where

- γ gyromagnetic ratio (>0),
- M total magnetization,
- H total effective magnetic field,
- α loss parameter (>0).

Now, it is assumed that the direction of a dc magnetic field H_i and a saturated magnetization M_s are in the z direction; furthermore, an alternating magnetic field h and an RF magnetization m is assumed to be much smaller than H_i, M_s, respectively:

$$\vec{M}=\begin{bmatrix} m_x \\ m_y \\ M_s \end{bmatrix} \qquad \vec{H}=\begin{bmatrix} h_x \\ h_y \\ H_i \end{bmatrix}. \tag{2}$$

Expanding (1) with M and H in (2) leads to

$$\frac{dm_x}{dt}=-\gamma(-M_s h_y+H_i m_y)-\alpha\frac{dm_y}{dt} \tag{3a}$$

$$\frac{dm_y}{dt}=-\gamma(M_s h_x-H_i m_x)+\alpha\frac{dm_x}{dt}. \tag{3b}$$

Rewriting the preceding equations yields

$$(1+\alpha^2)\frac{d^2m_x}{dt^2}+\omega_\tau\frac{dm_x}{dt}+\omega_i^2 m_x = \mu_0\omega_i\omega_m h_x+\mu_0\omega_{\alpha m}\frac{dh_x}{dt}+\mu_0\omega_m\frac{dh_y}{dt} \quad (4a)$$

$$(1+\alpha^2)\frac{d^2m_y}{dt^2}+\omega_\tau\frac{dm_y}{dt}+\omega_i^2 m_y = \mu_0\omega_i\omega_m h_y+\mu_0\omega_{\alpha m}\frac{dh_y}{dt}-\mu_0\omega_m\frac{dh_x}{dt} \quad (4b)$$

where

$$\omega_i=\gamma H_i \quad (4c)$$

$$\omega_m=\gamma M_s/\mu_0 \quad (4d)$$

$$\omega_\tau=2\alpha\omega_i \quad (4e)$$

$$\omega_{\alpha m}=\alpha\omega_m. \quad (4f)$$

The coupling between the variables of the different directions in the above equations is formulated as follows at the only node in which both combined components exist. At node E, the magnetic field components H_x, H_y, and the electric field E_z are related from Table I, so (4a) and (4b) can be used at node E, involving the coupling terms between H_x and H_y. And at node A, where H_x, H_z, and E_y are concerned, the following equation, in which the coupling term is removed from (4a), is related by

$$(1+\alpha^2)\frac{d^2m_x}{dt^2}+\omega_\tau\frac{dm_x}{dt}+\omega_i^2 m_x = \mu_0\omega_i\omega_m h_x+\mu_0\omega_{\alpha m}\frac{dh_x}{dt}. \quad (5)$$

This is also the case at node D, where H_y, H_z, and E_x are concerned. So the following equation, in which the coupling term is removed from (4b), is related by

$$(1+\alpha^2)\frac{d^2m_y}{dt^2}+\omega_\tau\frac{dm_y}{dt}+\omega_i^2 m_y = \mu_0\omega_i\omega_m h_y+\mu_0\omega_{\alpha m}\frac{dh_y}{dt}. \quad (6)$$

Thus, the equivalent circuit at every node in the ferrite is shown conceptually in Fig. 2, and a detailed conceptually equivalent circuit for node E is shown in Fig. 3. In this figure, the lumped inductances $\Delta L_x, \Delta L_y$ represent the noncoupling term in the equation, and the mutual coupling expression ΔM_{xy} shows the coupling term. For the steady state, the former and the latter correspond to the diagonal elements and the off-diagonal elements of the permeability tensor, respectively.

The description is mainly of the formulation at node E, which is directly concerned with the gyroanisotropy of ferrite caused by the coupling term in the characteristic equation. Before the formulation of (4) by the trapezoidal rule, the electromagnetic variables are transformed to equivalent circuit ones. This treatment yields the formulation of the unified nodal equation by use of the continuity law of currents. At node E, the following correspondences are arrived at from Table I:

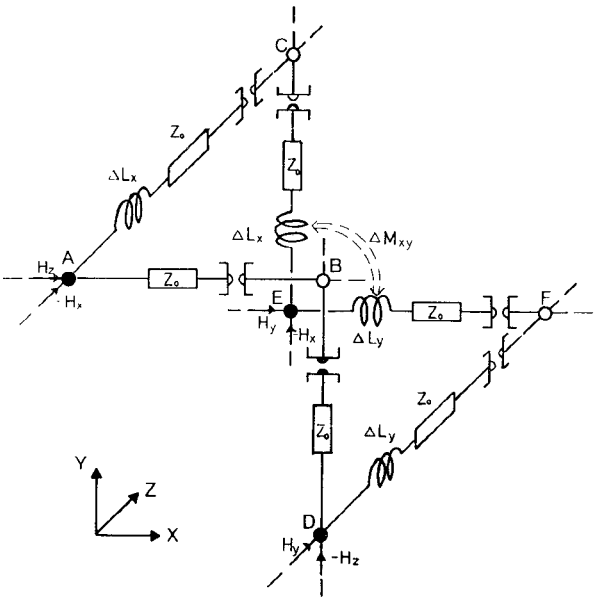

Fig. 2. Unit equivalent circuit of magnetized ferrite for dc magnetic field H_z.

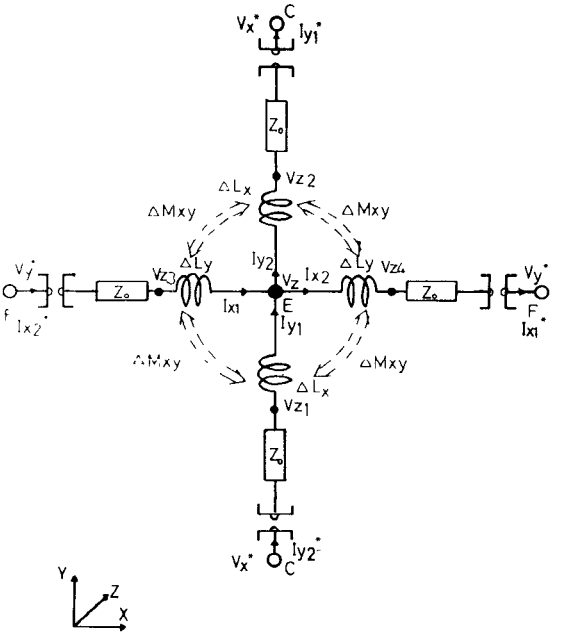

Fig. 3 Equivalent circuit at node $E(l, m, n)$ for dc magnetic field H_z.

$$V_z=-E_z \quad (7a)$$

$$I_y=-H_x \quad (7b)$$

$$I_x=H_y. \quad (7c)$$

Furthermore, new equivalent circuit variables J_y, J_x are defined for magnetization m_x, m_y, respectively. They obey the correspondences of the magnetic field, so the defini-

tions are similar to those of (7b) and (7c), and are given by

$$J_y = -m_x \tag{8a}$$

$$J_x = m_y. \tag{8b}$$

At the electric node E, the magnetic field corresponds to the current variables in each connected line, so that J_x, J_y mean the magnetic flux of the equivalent inductance shown in Fig. 3. Using (7) and (8), (4a) and (4b) are rewritten as follows, respectively:

$$\frac{d^2J_y}{dt} + k_\tau \frac{dJ_y}{dt} + k_i^2 J_y = k_{im} I_y + k_{\alpha m} \frac{dI_y}{dt} - k_m \frac{dI_x}{dt} \tag{9a}$$

$$\frac{d^2J_x}{dt} + k_\tau \frac{dJ_x}{dt} + k_i^2 J_x = k_{im} I_x + k_{\alpha m} \frac{dI_x}{dt} + k_m \frac{dI_y}{dt} \tag{9b}$$

where

$$k_\tau = \omega_\tau/(1+\alpha^2) \tag{9c}$$

$$k_i = \omega_i^2/(1+\alpha^2) \tag{9d}$$

$$k_{im} = \mu_0 \omega_i \omega_m/(1+\alpha^2) \tag{9e}$$

$$k_{\alpha m} = \mu_0 \omega_{\alpha m}/(1+\alpha^2) \tag{9f}$$

$$k_m = \mu_0 \omega_m/(1+\alpha^2). \tag{9g}$$

These equations are the second differential equations with respect to time t, so they can be transformed to the difference form by twice using the trapezoidal rule.

By a first application of the trapezoidal rule to (9a) and (9b) at time t, we obtain

$$K_y(t) = -\frac{k_i \Delta t}{2}\left(J_y(t) + J_y(t-\Delta t)\right) + \frac{k_{im}\Delta t}{2}\left(I_y(t) + I_y(t-\Delta t)\right) + K_y(t-\Delta t) \tag{10a}$$

$$K_x(t) = -\frac{k_i \Delta t}{2}\left(J_x(t) + J_x(t-\Delta t)\right) + \frac{k_{im}\Delta t}{2}\left(I_x(t) + I_x(t-\Delta t)\right) + K_x(t-\Delta t) \tag{10b}$$

where

$$K_y(t) = \frac{dJ_y(t)}{dt} + k_\tau J_y(t) - k_{\alpha m} I_y(t) + k_m I_x(t) \tag{10c}$$

$$K_x(t) = \frac{dJ_x(t)}{dt} + k_\tau J_x(t) - k_{\alpha m} I_x(t) - k_m I_y(t). \tag{10d}$$

Here, Δt is the time difference. A second application of the trapezoidal rule to (10a) and (10b) at time t, using (10a) and (10b) at time $t - \Delta t$, yields

$$\left(1 + k_\tau \frac{\Delta t}{2} + k_i \frac{\Delta t^2}{4}\right) J_y(t) - \left(k_{\alpha m} + k_{im}\frac{\Delta t}{2}\right)\frac{\Delta t}{2} I_y(t) + k_m \frac{\Delta t}{2} I_x(t)$$
$$= \left(1 - k_\tau \frac{\Delta t}{2} - k_i \frac{\Delta t^2}{4}\right) J_y(t-\Delta t) + \left(k_{\alpha m} + k_{im}\frac{\Delta t}{2}\right)\frac{\Delta t}{2} I_y(t-\Delta t) - k_m \frac{\Delta t}{2} I_x(t-\Delta t) + K_y(t-\Delta t)\Delta t \tag{11a}$$

$$\left(1 + k_\tau \frac{\Delta t}{2} + k_i \frac{\Delta t^2}{4}\right) J_x(t) - \left(k_{\alpha m} + k_{im}\frac{\Delta t}{2}\right)\frac{\Delta t}{2} I_x(t) - k_m \frac{\Delta t}{2} I_y(t)$$
$$= \left(1 - k_\tau \frac{\Delta t}{2} - k_i \frac{\Delta t^2}{4}\right) J_x(t-\Delta t) + \left(k_{\alpha m} + k_{im}\frac{\Delta t}{2}\right)\frac{\Delta t}{2} I_x(t-\Delta t) + k_m \frac{\Delta t}{2} I_y(t-\Delta t) + K_x(t-\Delta t)\Delta t. \tag{11b}$$

In this way, the second-order differential equations are changed to the first-order difference equations by definition of the variables K_y and K_x.

Next, in each connected line of the electric node, the time derivative of the flux J_y, J_x causes the voltage drop V_y, V_x in each inductance, respectively:

$$V_y(t) = \frac{dJ_y(t)}{dt} \tag{12a}$$

$$V_x(t) = \frac{dJ_x(t)}{dt}. \tag{12b}$$

Equations (12a) and (12b) are also transformed to the difference form by using the trapezoidal rule:

$$J_y(t) = \frac{\Delta t}{2}\left(V_y(t) + V_y(t-\Delta t)\right) + J_y(t-\Delta t) \tag{13a}$$

$$J_x(t) = \frac{\Delta t}{2}\left(V_x(t) + V_x(t-\Delta t)\right) + J_x(t-\Delta t) \tag{13b}$$

Finally, substituting (13a) and (13b) into (11a) and (11b), respectively, the difference equations of voltage–current characteristics of the magnetized ferrite on time domain are as follows:

$$D_1 V_y(t) - D_2 I_y(t) + D_3 I_x(t) = -D_1 V_y(t-\Delta t) + D_2 I_y(t-\Delta t) - D_3 I_x(t-\Delta t) - D_4 J_y(t-\Delta t) + D_5 K_y(t-\Delta t) \tag{14a}$$

$$D_1 V_x(t) - D_2 I_x(t) - D_3 I_y(t) = -D_1 V_x(t-\Delta t) + D_2 I_x(t-\Delta t) + D_3 I_y(t-\Delta t) - D_4 J_x(t-\Delta t) + D_5 K_x(t-\Delta t) \tag{14b}$$

where

$$D_1 = \left(1 + k_\tau \frac{\Delta t}{2} + k_\iota \frac{\Delta t^2}{4}\right)\frac{\Delta t}{2} \tag{14c}$$

$$D_2 = \left(k_{\alpha m} + k_{\iota m}\frac{\Delta t}{2}\right)\frac{\Delta t}{2} \tag{14d}$$

$$D_3 = k_m \frac{\Delta t}{2} \tag{14e}$$

$$D_4 = k_\tau \Delta t + k_\iota \frac{\Delta t^2}{2} \tag{14f}$$

$$D_5 = \Delta t. \tag{14g}$$

From equations (14), the inductance in Fig. 3 is defined as $\Delta L_x = \Delta L_y = D_2/D_1$ and the conceptual mutual inductance $\Delta M_{xy} = D_3/D_1$ is expressed by the arrow mark. In this expression, the gyroanisotropy is represented by the difference in sign between the third term on the left side of (14a) and (14b).

IV. Nodal Equations and Equivalent Circuit

In Section III, the equation of motion of ferrite is transformed to the difference equations using the equivalent variables relative to magnetization: J_x, J_y, and K_x, K_y. The definition of these variables makes it possible to complete the iterative computation on the time domain by use of the values obtained only at the previous time step. In this section, these equations are combined with Bergeron's formulation of the one-dimensional line in the three-dimensional network described in Section II. The time difference Δt coincides with the transit time between two adjacent nodes in the lattice network. The connection of four lines is shown in Fig. 3. As shown in the figure, by using the voltage variables V_{z1}, V_{z2}, V_{z3}, and V_{z4} in each line, the voltage drop of each inductance for (13a), (13b) is given by

$$V_{y1}(t) = V_{z1}(t) - V_z(t) \tag{15a}$$

$$V_{y2}(t) = V_z(t) - V_{z2}(t) \tag{15b}$$

$$V_{x1}(t) = V_{z3}(t) - V_z(t) \tag{15c}$$

$$V_{x2}(t) = V_z(t) - V_{z4}(t) \tag{15d}$$

where $V_z(t)$ is the voltage of node E. It is assumed that the quantities of the variables of each coupling term in (14) are as follows. The current variable I_x in the x direction in (14a) is given by

$$I_x(t) = I_{x1}(t) + I_{x2}(t). \tag{16a}$$

Similarly, for I_y in the y direction in (14b),

$$I_y(t) = I_{y1}(t) + I_{y2}(t). \tag{16b}$$

Substituting (15a)–(15d) into (14a)–(14b) by considering (16a), (16b), the difference equations for each inductance are as follows:

$$\begin{aligned} &D_1(V_{z1}(t) - V_z(t)) - D_2 I_{y1}(t) + D_3 I_x(t) \\ &\quad = -D_1 V_{y1}(t-\Delta t) + D_2 I_{y1}(t-\Delta t) - D_3 I_x(t-\Delta t) \\ &\qquad - D_4 J_{y1}(t-\Delta t) + D_5 K_{y1}(t-\Delta t) \end{aligned} \tag{17a}$$

$$\begin{aligned} &D_1(V_z(t) - V_{z2}(t)) - D_2 I_{y2}(t) + D_3 I_x(t) \\ &\quad = -D_1 V_{y2}(t-\Delta t) + D_2 I_{y2}(t-\Delta t) - D_3 I_x(t-\Delta t) \\ &\qquad - D_4 J_{y2}(t-\Delta t) + D_5 K_{y2}(t-\Delta t) \end{aligned} \tag{17b}$$

$$\begin{aligned} &D_1(V_{z3}(t) - V_z(t)) - D_2 I_{x1}(t) - D_3 I_y(t) \\ &\quad = -D_1 V_{x1}(t-\Delta t) + D_2 I_{x1}(t-\Delta t) + D_3 I_y(t-\Delta t) \\ &\qquad - D_4 J_{x1}(t-\Delta t) + D_5 K_{x1}(t-\Delta t) \end{aligned} \tag{17c}$$

$$\begin{aligned} &D_1(V_z(t) - V_{z4}(t)) - D_2 I_{x2}(t) - D_3 I_y(t) \\ &\quad = -D_1 V_{x2}(t-\Delta t) + D_2 I_{x2}(t-\Delta t) + D_3 I_y(t-\Delta t) \\ &\qquad - D_4 J_{x2}(t-\Delta t) + D_5 K_{x2}(t-\Delta t). \end{aligned} \tag{17d}$$

On the other hand, Bergeron's expression of each transmission line at node $E(l, m, n)$ is given by

$$\begin{aligned} &V_{z1}(l,m,n,t) + z_0 I_{y1}(l,m,n,t) \\ &\quad = I_{y2}^*(l,m-1,n,t-\Delta t) + z_0 V_x^*(l,m-1,n,t-\Delta t) \end{aligned} \tag{18a}$$

$$\begin{aligned} &V_{z2}(l,m,n,t) - z_0 I_{y2}(l,m,n,t) \\ &\quad = I_{y1}^*(l,m+1,n,t-\Delta t) - z_0 V_x^*(l,m+1,n,t-\Delta t) \end{aligned} \tag{18b}$$

$$\begin{aligned} &V_{z3}(l,m,n,t) + z_0 I_{x1}(l,m,n,t) \\ &\quad = I_{x2}^*(l-1,m,n,t-\Delta t) + z_0 V_y^*(l-1,m,n,t-\Delta t) \end{aligned} \tag{18c}$$

$$\begin{aligned} &V_{z4}(l,m,n,t) - z_0 I_{x2}(l,m,n,t) \\ &\quad = I_{x1}^*(l+1,m,n,t-\Delta t) - z_0 V_y^*(l+1,m,n,t-\Delta t) \end{aligned} \tag{18d}$$

where the parameters l, m, and n denote the described position numbers in the x, y, and z directions, respectively. And z_0 is the characteristic impedance of the line at the electric node. Substituting (18a)–(18d) into (17a)–(17d) and eliminating V_{z1}, V_{z2}, V_{z3}, and V_{z4}, the following equations were obtained. For simplicity, the position parameters l, m, and n are omitted in these equations:

$$D_1 V_z(t) + (z_0 D_1 + D_2) I_{y1}(t) - D_3 I_x(t) = D_1 A_1 - E_1 \tag{19a}$$

$$D_1 V_z(t) - (z_0 D_1 + D_2) I_{y2}(t) + D_3 I_x(t) = D_1 A_2 + E_2 \tag{19b}$$

$$D_1 V_z(t) + (z_0 D_1 + D_2) I_{x1}(t) + D_3 I_y(t) = D_1 A_3 - E_3 \tag{19c}$$

$$D_1 V_z(t) - (z_0 D_1 + D_2) I_{x2}(t) - D_3 I_y(t) = D_1 A_4 + E_4 \tag{19d}$$

where E_1-E_4 correspond to the right side of (17a)–(17d), and A_1-A_4 correspond to the right side of (18a)–(18d), respectively. These quantities are evaluated from values computed at a previous time step of the iterative procedure. By subtracting (19b) from (19a), and (19d) from (19c), the equations about I_x in (16a) and I_y in (16b) can be obtained, respectively. Whereas (19a)–(19d) become

$$D_1V_z(t)+(z_0D_1+D_2)I_{y1}(t)=D_1A_1-E_1+D_3I_x(t) \tag{20a}$$

$$D_1V_z(t)-(z_0D_1+D_2)I_{y2}(t)=D_1A_2+E_2-D_3I_x(t) \tag{20b}$$

$$D_1V_z(t)+(z_0D_1+D_2)I_{x1}(t)=D_1A_3-E_3-D_3I_y(t) \tag{20c}$$

$$D_1V_z(t)-(z_0D_1+D_2)I_{x2}(t)=D_1A_4+E_4+D_3I_y(t). \tag{20d}$$

The continuity of the current at node $E(l, m, n)$ is given by

$$I_{y1}(t)-I_{y2}(t)+I_{x1}(t)-I_{x2}(t)=0. \tag{21}$$

Substituting (20a)–(20d) into (21), the unified nodal equation at the time t is given by

$$V_z(l,m,n,t)=\frac{\psi_1+\psi_2+\psi_3+\psi_4}{4D_1} \tag{22}$$

where ψ_1, ψ_2, ψ_3, and ψ_4 correspond to the right side of (20a)–(20d), respectively. Each component of the currents at the time t is calculated by substituting $V_z(t)$ in (22) into (20a)–(20d), respectively:

$$I_{y1}(t)=(\psi_1-D_1V_z(t))/(z_0D_1+D_2) \tag{23a}$$

$$I_{y2}(t)=-(\psi_2-D_1V_z(t))/(z_0D_1+D_2) \tag{23b}$$

$$I_{x1}(t)=(\psi_3-D_1V_z(t))/(z_0D_1+D_2) \tag{23c}$$

$$I_{x2}(t)=-(\psi_4-D_1V_z(t))/(z_0D_1+D_2). \tag{23d}$$

Similarly, $V_{z1}(t)$–$V_{z4}(t)$ are computed by substituting (23a)–(23d) into (18a)–(18d). Also, $J_{y1}(t)$, $J_{y2}(t)$, $J_{x1}(t)$, and $J_{x2}(t)$ are evaluated by substituting $V_z(t)$ and $V_{z1}(t)$–$V_{z4}(t)$ into (13a)–(13b) using (15a)–(15d), respectively. Finally, $K_{y1}(t)$, $K_{y2}(t)$, $K_{x1}(t)$, and $K_{x2}(t)$ are obtained by substituting $I_{y1}(t)$, $I_{y2}(t)$, $I_{x1}(t)$, $I_{x2}(t)$, $J_{y1}(t)$, $J_{y2}(t)$, $J_{x1}(t)$, and $J_{x2}(t)$ into (10a)–(10b). At each node E, the computation is performed, in this same procedure, for each time step. At node A and node D, the resultant formulations correspond to the noncoupling condition of that at node E. Then the time response of the field in the overall region is evaluated by the iterative procedure at each node, in a manner similar to that at node E.

In this analysis, the direction of the dc magnetic field is supposed to be the z direction, but for the case where the dc magnetic field is in the other direction, the equivalent circuit and the formulation are similarly brought about.

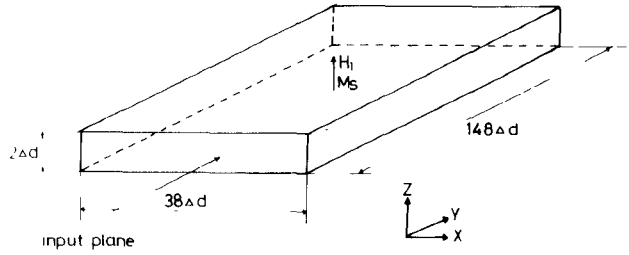

Fig. 4. Analyzed model of rectangular waveguide filled with ferrite.

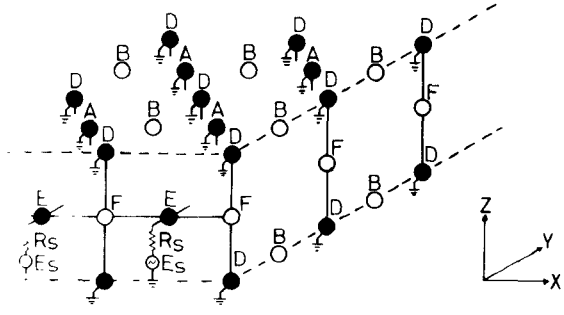

Fig. 5. Equivalent circuit of the surface of the waveguide and the input condition, where R_s is the characteristic impedance of the waveguide and E_s is the voltage source.

V. Numerical Results and Discussion

To examine the validity of the formulation described in the preceding section, two examples are taken with respect to the relative angles between the directions of the dc magnetic field and the wave propagation.

The first case is that where the angle is 90°. The characteristic of λ versus σ is computed for various p. Here, λ is the wavelength in the perpendicularly magnetized rectangular waveguide filled with the ferrite shown in Fig. 4. The length in the x direction is $38\Delta d$; in the y direction it is $148\ \Delta d$, and in the z direction it is $2\Delta d$. The thin structure of the z direction yields only the propagation of the TE wave on the xy plane. Here σ is the ratio of the natural precession frequency to the signal frequency, and p is the ratio of the frequency associated with the saturation magnetization to the signal frequency. The wall of the waveguide is supposed to have infinite conductivity. So the equivalent circuit in the present method for the surface of the conductor is realized by 1) short-circuiting the node on the surface, in which the tangential component of the electric field or the normal component of the magnetic field corresponds to the voltage variable and 2) open-circuiting the node on the surface, in which the preceding electromagnetic component corresponds to the current variable as shown in Fig. 5. The input of the sinusoidal wave is applied in each E node in the input DEF plane, which includes the D, E, and F nodes shown in Fig. 5. The wavelength λ_0 of the input wave is $75\Delta d$ in free space. The mode of the input wave is assumed to be the TE_{10} mode. The output plane is terminated by the characteristic impedance of the TE_{10} mode to approximate the matching condition. Using this model, the results obtained are as shown in Fig. 6, where the dielectric constant

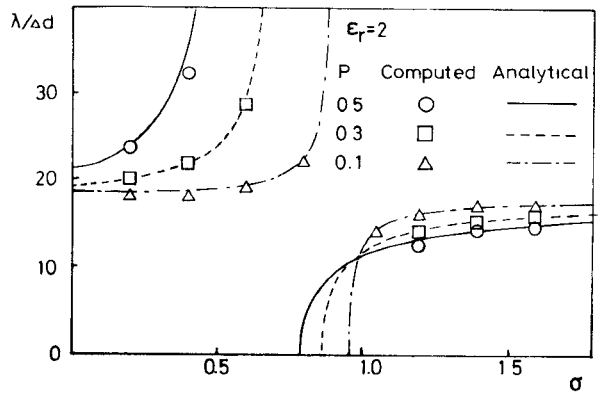

Fig. 6. Characteristic of λ versus σ for various p, where λ is the wavelength, σ is the ratio of the natural precession frequency to the signal frequency, and p is the ratio of the frequency associated with the saturation magnetization to the signal frequency.

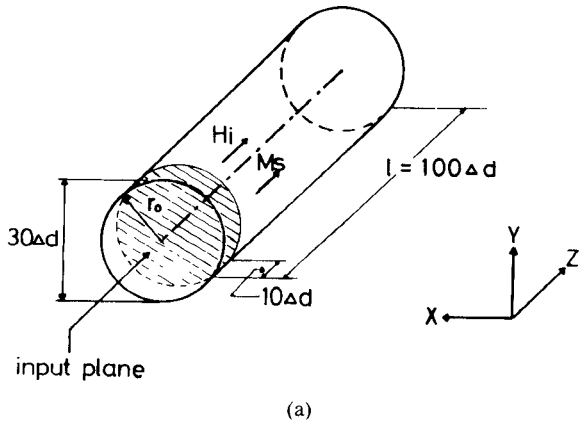

(a)

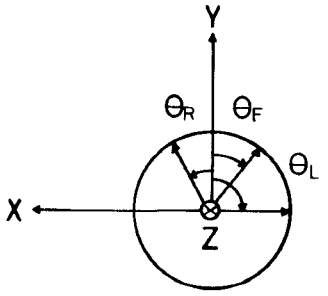

(b)

Fig. 7. (a) Analyzed model of cylindrical waveguide filled with ferrite (b) Coordinate system of angle of rotation θ_L for L-wave, θ_R for R-wave, and θ_F for linear polarization.

ϵ_r is fixed to be 2, and σ is changed under three parameters of p. The analytical curves of wavelength are calculated by using μ_{eff}, which is determined from given σ and p by the following formula:

$$\lambda = \frac{\lambda_0/\sqrt{\epsilon_r \mu_{\text{eff}}}}{\sqrt{1-\left(\frac{\lambda_0}{\sqrt{\epsilon_r \mu_{\text{eff}}}\lambda_c}\right)^2}}$$

where

$$\mu_{\text{eff}} = \frac{\mu_r^2 - \kappa_r^2}{\mu_r}.$$

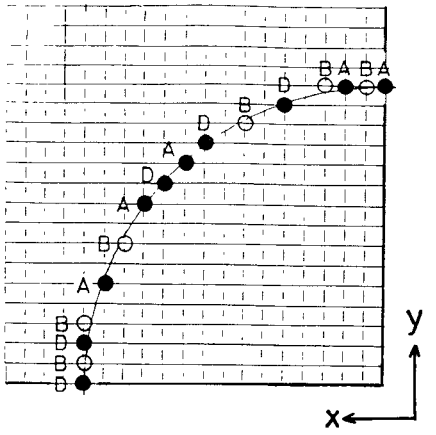

(a)

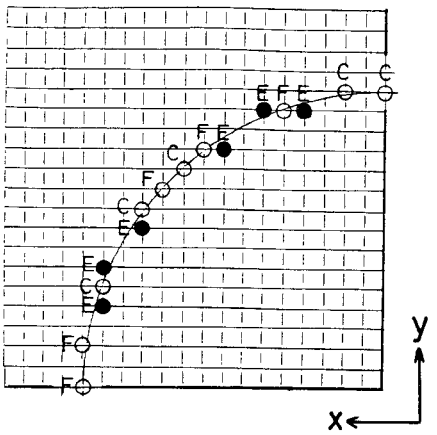

(b)

Fig. 8 Arrangement of nodes on wall of cylindrical waveguide. (a) *ABD* plane (b) *CEF* plane.

From the above description, the present method uses only primary parameters σ and p for the medium condition of ferrite. The good agreement in Fig. 6 of the computed wavelength with analytical ones shows the validity of the formulation. At steady state, the simulation presents the effect of σ and p as the effective permeability μ_{eff}. The secondary parameters μ_r and κ_r are also involved in the computation.

Next, the Faraday effect was simulated by a cylindrical waveguide containing ferrite. Fig 7(a) shows the analyzed model of the cylindrical waveguide. The direction of the dc magnetic field is the same longitudinal direction as the propagation. The radius of the waveguide is $r_0 = 15\Delta d$, and the longitudinal length in the z direction $l = 100\Delta d$. Fig. 7(b) shows the coordinate system for the angle of the plane of the polarization θ_L, θ_R, and θ_F along the z direction for the L-wave, the R-wave, and the linear polarization, respectively. The boundary conditions of the wall also have perfect conductivity, and in Fig. 8, the arrangements of the nodes on a quarter of the wall of the waveguide are shown by the cross section of both the *ABD* and *CEF* planes. The curve is approximated as stairs because of the cubical lattice network. For simplicity a detailed description of the treatment of these boundary conditions is not given. The

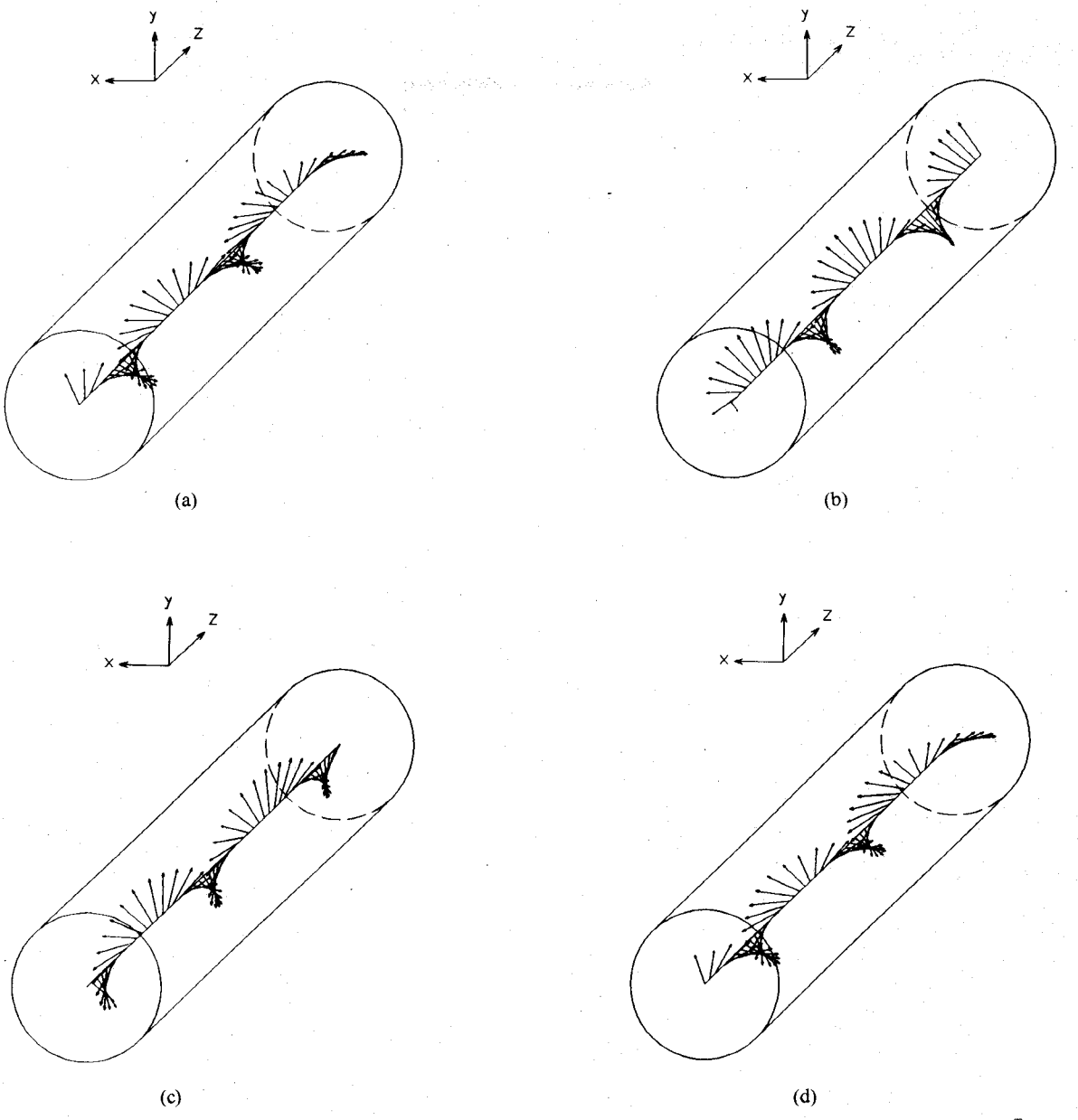

Fig. 9. Time variation of electric field distribution of L-wave on central axis of waveguide. (a) $t = t_0$. (b) $t = t_0 + \frac{T}{3}$. (c) $t = t_0 + \frac{2}{3}T$. (d) $t = t_0 + T$.

input of the sinusoidal wave is applied in the input plane of ABD, and the mode of the input wave is assumed to be the TE_{11} mode. So the component E_y of the TE_{11} mode is applied at node A_n with correspondent amplitude distribution at the node. In similar fashion, E_x is also applied at node D_n. The R-wave and the L-wave are generated by shifting the phase of the E_x and E_y components of the input plane. The output plane is terminated by the characteristic impedance of the TE_{11} mode to appropriate the matching condition.

Using this model, transient analysis is performed to show the process of Faraday rotation. In this case, the parameters of the ferrite are given by $\sigma(=\omega_i/\omega) = 0.8$, $p(=\omega_m/\omega) = 0.09$, and $\alpha = 0$. T, which shows the period of the applied wave, is $150\Delta t$. This size of division, for the size of the cylindrical waveguide and the period of the applied sinusoidal wave, is sufficient for good resolution in space and time. The input is applied at $t = 0$.

Figs. 9, 10, and 11 shows the instantaneous time variation of the rotation of the electric field for a period on the central axis for the input of the L-wave, the R-wave, and the linear polarization, respectively. As shown in Figs. 9 and 10, the electric field rotates to the left and the right, respectively, as the propagation distance in the z direction increases. In Fig. 11, the resultant rotation of linear polarization is observed, which is caused by the composition of the L-wave and R-wave. These phenomena are supposed to be the effect of Faraday rotation. Theoretically, under

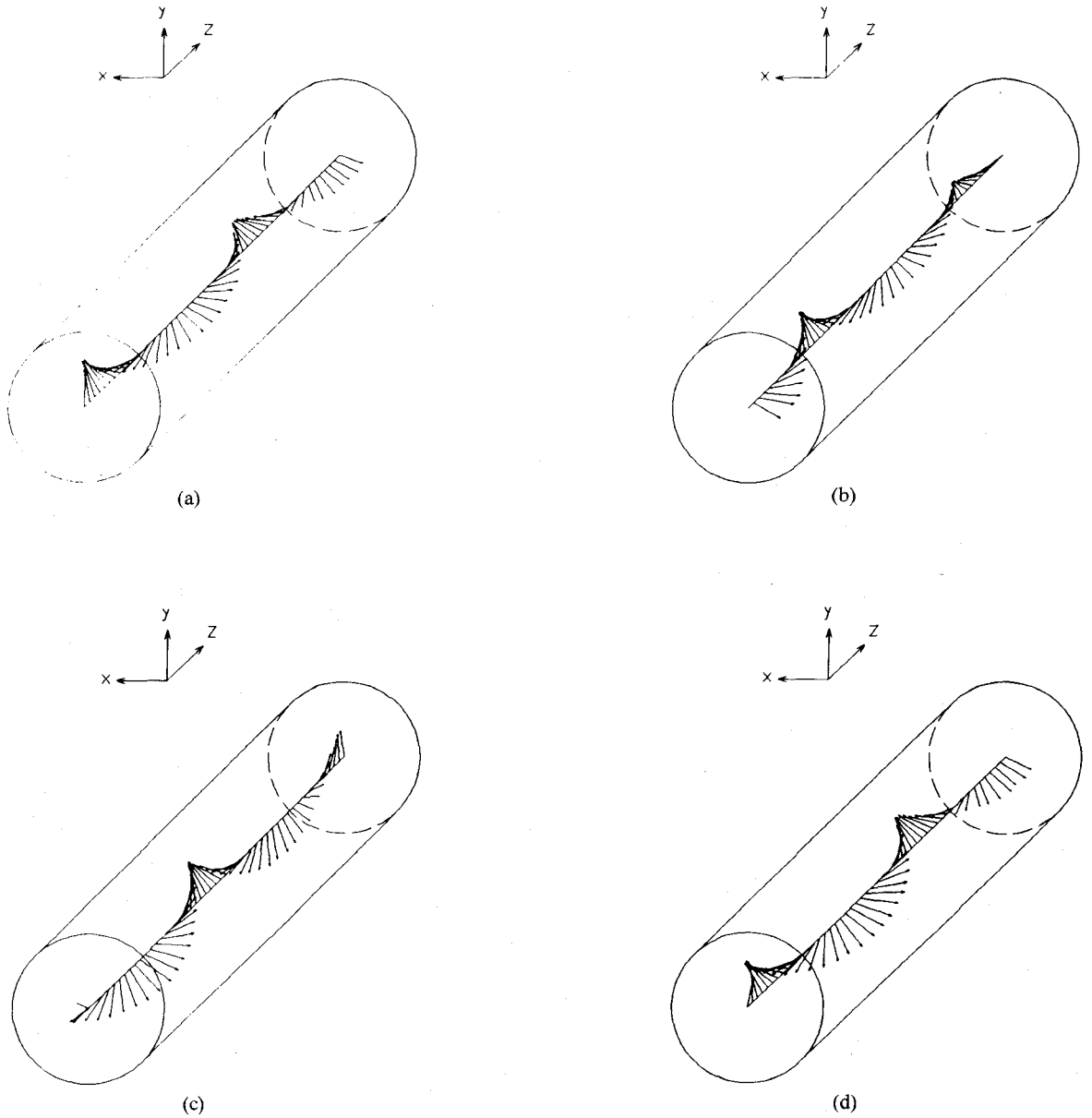

Fig. 10. Time variation of electric field distribution of R-wave on central axis of waveguide. (a) $t = t_0$. (b) $t = t_0 + \frac{T}{3}$. (c) $t = t_0 + \frac{2}{3}T$. (d) $t = t_0 + T$.

conditions of actual use, the refractive index for the R-wave is smaller than that of the L-wave, so the phase velocity of the R-wave is larger than that of the L-wave. Therefore, θ_F should rotate to the right as the propagation distance in the z direction increases, as shown Fig. 11. On the other hand, Fig. 12 shows the time variation of the instantaneous pattern of the electric field in the cross sections. The observed plane is denoted by the slanted lines in Fig. 7(a). In these figures, the rotation of the TE_{11} mode is shown. At each position on the z axis, the above condition causes the elliptical polarization that rotates to the right. Furthermore, to ascertain the realization of the Faraday rotation, there is an investigation into the composition of the L-wave and the R-wave of circular polarization that causes the rotation of the linear polarization. Fig. 13 shows the variation of the angles θ_L and θ_R of the electric field of the L-wave and the R-wave versus the propagation distance along the z axis at $t = t_0$ as shown in Figs. 9 and 10, respectively. The angles θ_L and θ_R are in good proportion to the propagation distance, and the phase velocity of the L-wave is smaller than that of the R-wave. These results show that the propagation characteristics of the L-wave and R-wave are well calculated. When comparing the line of $(\theta_L - \theta_R)/2$ with plotted points of θ_F, they are in close agreement. For the Faraday rotation, the points of the maximum amplitude occur theoretically at the condition of $(\theta_L + \theta_R)/2 = 180n$ (n: integer). In this figure, this characteristic is also observed for each plotted points of θ_F.

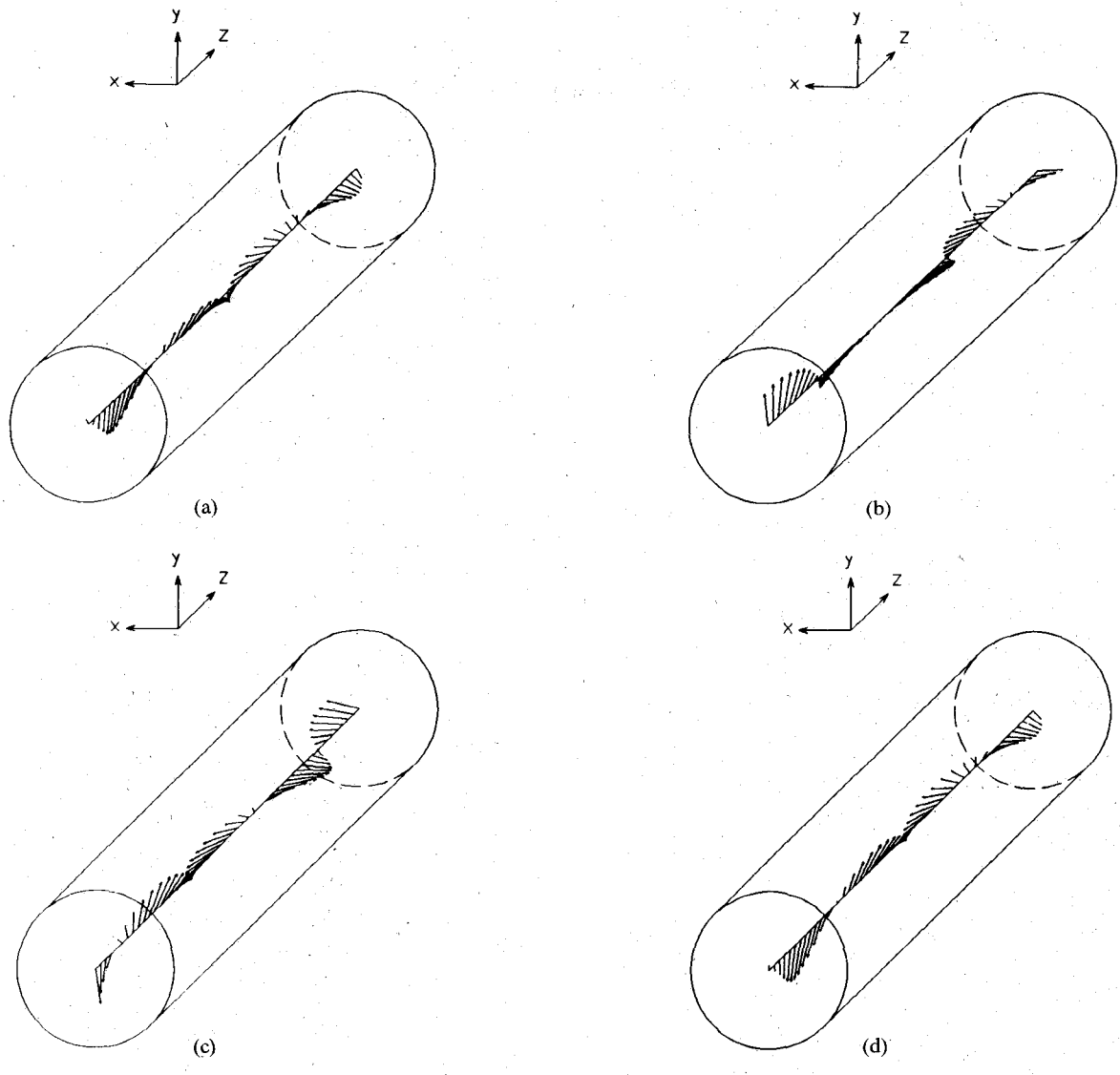

Fig. 11. Time variation of electric field distribution of linear polarization on central axis of waveguide. (a) $t = t_0$. (b) $t = t_0 + \frac{T}{3}$. (c) $t = t_0 + \frac{2}{3}T$. (d) $t = t_0 + T$.

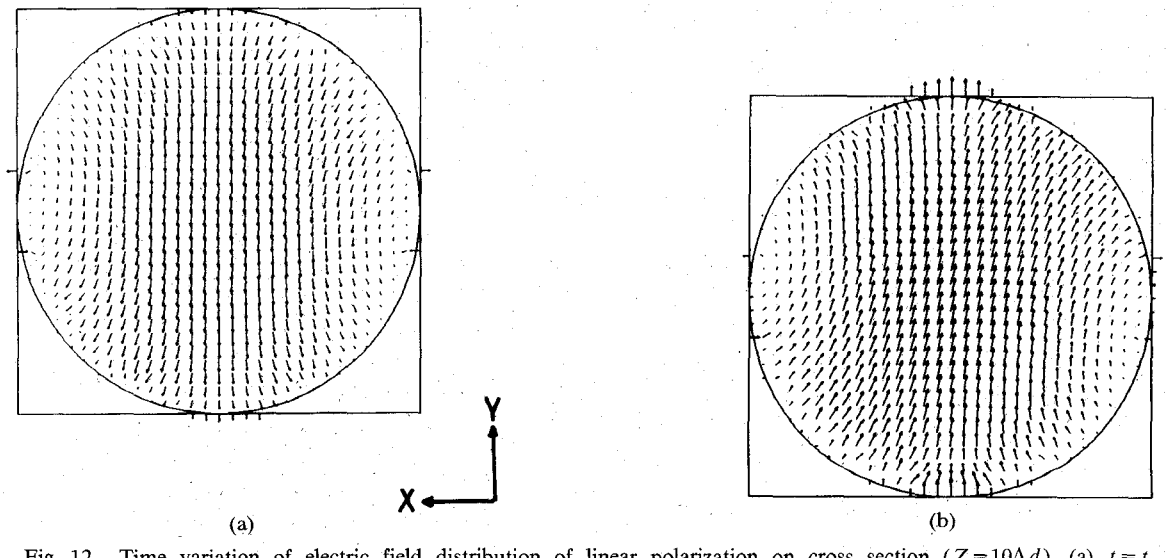

Fig. 12. Time variation of electric field distribution of linear polarization on cross section ($Z = 10\Delta d$). (a) $t = t_0$. (b) $t = t_0 + \frac{T}{3}$. (c) $t = t_0 + \frac{2}{3}T$. (d) $t = t_0 + T$.

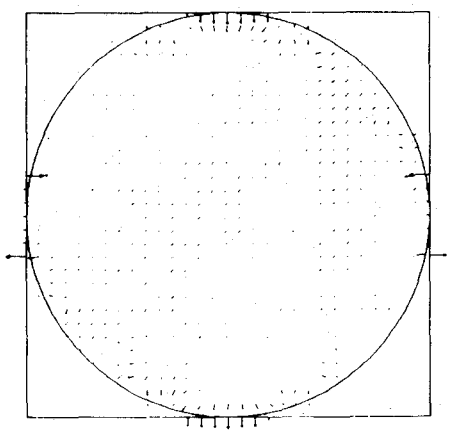

(c)

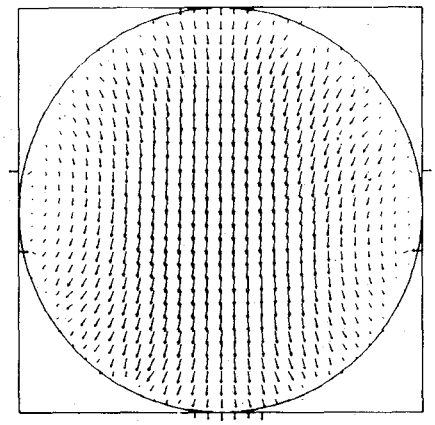

(d)

Fig. 12. continued

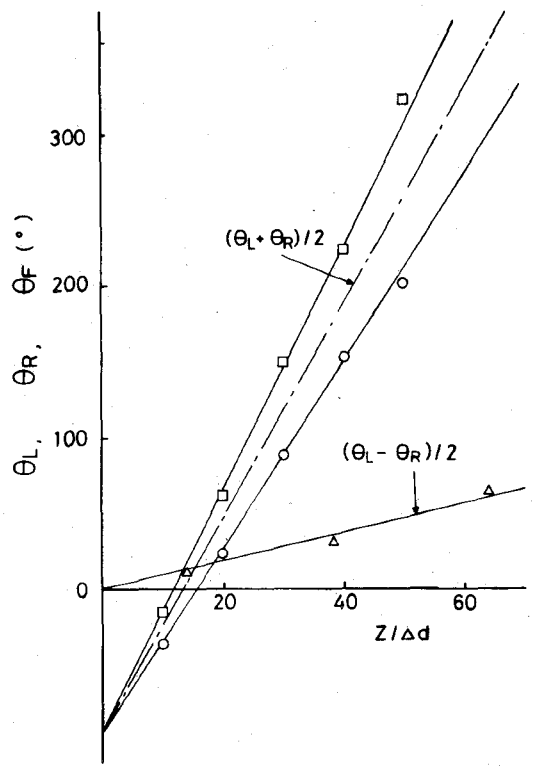

Fig. 13. Angle of rotation θ_L, θ_R, and θ_F versus propagation distance.

Finally, there is an investigation into the phase constants in the parameters used. For these conditions, the analytically obtained value of the phase constant β/β_0 of the L-wave and the R-wave are 1.696 and 1.291, respectively [11]. On the other hand, almost the same values are obtained in this analysis. So, by these considerations, it can be concluded that the Faraday effect of ferrite is simulated by the present method.

VI. Conclusions

The fundamental formulation of the magnetized ferrite in three-dimensional space and time domain by Bergeron's method is described. And the validity of this treatment is shown by two cases according to the angle between the directions of the dc magnetic field and the propagation of a wave. In these analyses, the important cases of the specific direction of the magnetic field, such as perpendicular and longitudinal to the direction of wave propagation, are studied, but the formulation for the optional direction can be performed in a similar manner. Furthermore, for the example analyzed, only sinusoidal excitation is used in making comparisons with the analytical results, but the formulation in this paper is a full-wave one on the time axis. So this formulation can be easily applied to microwave ferrite devices for high-speed pulse waves, which will become more important with the development of digital technology. We are applying this treatment to many kinds of nonreciprocal devices, among them circulators and isolators, using ferrite involving complicated boundary conditions, and studying transient properties for the high-speed pulse waves in the MIC. These results will be reported in later papers.

Acknowledgment

The authors gratefully acknowledge the valuable discussions with T. Kashiwa.

References

[1] N. Yoshida, I. Fukai, and J. Fukuoka, "Transient analysis of two-dimensional Maxwell's equations by Bergeron's method," *Trans. IECE Japan*, vol. J62-B, pp. 511–518, June 1979.

[2] N. Yoshida, I. Fukai, and J. Fukuoka, "Transient analysis of three-dimensional electromagnetic fields by nodal equations," *Trans. IECE Japan*, vol. J63-B, pp. 876–883, Sept. 1980.

[3] N. Yoshida and I. Fukai, "Transient analysis of a stripline having a corner in three-dimensional space," *IEEE Trans. Microwave Theory Tech.*, vol. MTT-32, pp. 491–498, May 1984.

[4] S. Koike, N. Yoshida, and I. Fukai, "Transient analysis of a directional coupler using a coupled microstrip slot line in three-dimensional space," *IEEE Trans. Microwave Theory Tech.*, vol. MTT-34, pp. 353–357, Mar. 1986.

[5] T. Aoto, N. Yoshida, and I. Fukai, "Transient analysis of the electromagnetic field for a wave absorber in three-dimensional space," *IEEE Trans. Electromagn. Compat.*, vol. EMC-29, Feb. 1987.

[6] N. Kukutsu, T. Kashiwa, N. Yoshida, and I. Fukai, "Fundamental treatment of anisotropic medium by Bergeron's method," *Trans. IECE Japan*, vol. J69-C, no. 12, pp. 1557–1559, Dec. 1986.

[7] K. S. Yee, "Numerical solution of initial boundary value problems involving Maxwell's equations in isotropic media," *IEEE Trans. Antennas Propagat.*, vol. AP-14, no. 3, pp. 302–307, May 1966.
[8] S. Akhtarzad and P. B. Johns, "Generalized elements for TLM method of numerical analysis," *Proc. Inst. Elec. Eng.*, vol. 122, pp. 1349–1352, Dec. 1975.
[9] P. B. Johns and M. O'Brien, "Use of the transmission-line modelling (t.l.m.) method to solve non-linear lumped networks," *Radio Electron. Eng.*, vol. 50, pp. 59–70, Jan./Feb. 1980.
[10] N. Yoshida, I. Fukai, and J. Fukuoka, "Application of Bergeron's method to anisotropic media," *Trans. IECE Japan*, vol. J64-B, pp. 1242–1249, Nov. 1981.
[11] R. A. Waldron, "Electromagnetic wave propagation in cylindrical waveguides containing gyromagnetic media," *J. Brit. Inst. Radio Eng.*, pp. 597–612, Oct. 1958; pp. 677–690, Nov. 1958; and pp. 733–746, Dec. 1958.

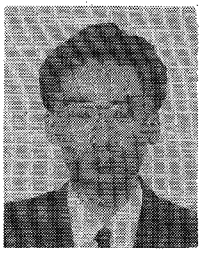

Naoya Kukutsu was born in Hokkaido, Japan, on September 16, 1962. He received the B.E. degree in electrical engineering from Hokkaido University, Sapporo, Japan, in 1986. He is presently working towards the M.E. degree in electrical engineering at the same university. He is now interested in the transient analysis of nonreciprocal MIC devices in three-dimensional space.

Mr. Kukutsu is an associate member of the Institute of Electronics, Information and Communication Engineers in Japan.

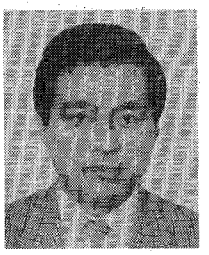

Norinobu Yoshida (M'87) was born in Hokkaido, Japan, on May 27, 1942. He received the B.E. and M.E. degrees in electronics engineering from Hokkaido University, Sapporo, Japan, in 1965 and 1967, respectively, and received the D.E. degree in electrical engineering from the same university in 1982.

He joined the Nippon Electric Company, Ltd., Tokyo, in 1967, and worked in computer-aided design in the Integrated Circuit Division. He became a Research Assistant in 1969 in the Department of Electrical Engineering on the Faculty of Engineering of Hokkaido University. He became a Lecturer in 1983 and an Associate Professor in 1984 in the same department. He presently is engaged in research on numerical methods for transient analysis of electromagnetic fields.

Dr. Yoshida is a member of the Institute of Electrical Engineers of Japan and the Institute of Electronics, Information and Communication Engineers in Japan.

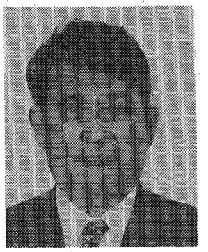

Ichiro Fukai (M'87) was born in Hokkaido, Japan, on August 21, 1930. He received the B.E., M.E., and D.E. degrees in electrical engineering from Hokkaido University, Sapporo, Japan, in 1953, 1956, and 1976, respectively.

In 1956, he joined the Defense Agency Technical Research and Development Institute. He became a Research Assistant in 1959 on the Faculty of Engineering of Hokkaido University and an Associate Professor at the Technical Teacher's Training Institute in 1961. In 1968 he became an Associate Professor and in 1977 a Professer in the Department of Electrical Engineering on the Faculty of Engineering at the same university.

Dr. Fukai is a member of the Institute of Electrical Engineers of Japan, and the Institute of Electronics, Information and Communication Engineers in Japan.